LA-UR-15-22110
Approved for public release; distribution is unlimited.

Title: Numerical computation of Pop plot

Author(s): Menikoff, Ralph

Intended for: Report

Issued: 2015-03-23

Numerical computation of Pop plot

Ralph Menikoff

March 9, 2015

Abstract

The Pop plot — distance-of-run to detonation versus initial shock pressure — is a key characterization of shock initiation in a heterogeneous explosive. Reactive burn models for high explosives (HE) must reproduce the experimental Pop plot to have any chance of accurately predicting shock initiation phenomena. This report describes a methodology for automating the computation of a Pop plot for a specific explosive with a given HE model. Illustrative examples of the computation are shown for PBX 9502 with three burn models (SURF, WSD and Forest Fire) utilizing the `xRage` code, which is the Eulerian ASC hydrocode at LANL. Comparison of the numerical and experimental Pop plot can be the basis for a validation test or as an aid in calibrating the burn rate of an HE model. Issues with calibration are discussed.

1 Introduction

A key characterization of shock initiation in a heterogeneous explosive is the distance-of-run to detonation as a function of the initial shock pressure. Ramsay and Popolato [1965] first observed that on a log-log scale the data is well represented by a straight line. This representation of shock initiation data is known as a Pop plot.

The Pop plot is obtained from a series of shock-to-detonation transition (SDT) experiments. Each experiment gives a single data point on the Pop plot. Originally, an explosive plane wave lens was used to drive the initial shock in a wedge shaped sample of high explosive (HE); see [Gibbs and Popolato, 1980, part II, sec 4.1]. A more modern technique utilizes a projectile from a gas gun to drive the initial HE shock; see [Gustavsen et al., 2002]. In both types of experiment, the flow in the region of interest is one-dimensional. Pop plot data are available for many explosives; see for example, [Gibbs and Popolato, 1980]. For less common explosives, the Pop plot may be the only shock initiation data available.

To utilize a reactive burn model to simulate shock initiation phenomena, at the very least, the model must reproduce the Pop plot. For a specific explosive, comparing the numerically generated Pop plot with experimental data can be used as a validation test. Pop plot data can also be used to partially calibrate a burn model. In this report, we describe a methodology for automating the computation of a Pop plot for a specific explosive with a given HE model. This has been implemented utilizing the `xRage` code, which is the Eulerian ASC hydrocode at LANL.

One notable aspect is the method for determining the distance-of-run to detonation. It employs the shock detector algorithm utilized by the SURF model. Results are shown for three HE models that have been used with PBX 9502; SURF, WSD and Forest Fire. For the latter two models, the shock detector is used only for output; *i.e.*, it does not affect the simulation, and in this respect is analogous to tracer particle output.

Also discussed are issues related to using Pop plot data to calibrate an HE burn model. All three models were previously calibrated to fit the Pop plot data. For other shock initiation simulations, the predictions of the different models can be different. Thus, fitting Pop plot data is necessary but not sufficient for a predictive model.

2 SDT simulation setup

For a point on the Pop plot, we setup a simulation that is the analog to a gas gun experiment; see figure 1. With an inflow boundary condition on the left, the projectile impact generates a sustained shock that drives the shock-to-detonation transition in the HE.

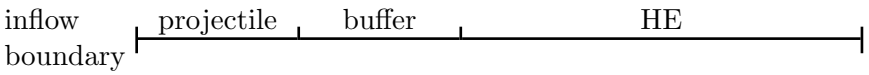

Figure 1: Sketch of the setup for a 1-D shock-to-detonation transition simulation. The projectile is given an initial velocity, while the buffer and HE are at rest.

Typical an initial velocity discontinuity results in a numerical glitch on startup. This is due to an entropy error from the numerical transient when a shock profile is formed or changes; see [Menikoff, 1994]. A buffer material is introduced between the projectile and the HE so that the startup-error does not affect the burning in the HE.

A similar numerical glitch or entropy error also arises due to the shock impedance match at the buffer/HE interface. To eliminate this glitch, the projectile and buffer are chosen to be inert materials with the same equation of state (EOS) as the HE reactants. In addition, the same grid resolution is needed for the buffer and HE. Otherwise, the shock profiles in the buffer and HE would have different numerical widths, and the shock propagation would be disturbed at the interface.

With the same materials, the projectile impact generates a shock in the buffer with a particle velocity of half the projectile velocity. The projectile velocity can be selected based on the shock Hugoniot for the HE reactants to give a point on the Pop plot with the desired shock pressure.

3 Determination of run distance

Experimentally, the trajectory of the lead shock $x(t)$ is measured. Initiation of a detonation wave results in a rapid increase in wave speed; from shock velocity to detonation velocity. The wave velocity determined by finite differences of the data is very noisy. Instead, a functional form is used to fit the

trajectory and then the wave velocity is determined by analytically taking the derivative of the fitting form; see for example [Hill and Gustavsen, 2002]. In effect, the fitting form is used to smooth the data. The distance-of-run to detonation is then determine by a simple criterion, such as the point of maximum acceleration.

A numerical simulation provides a lot more information on the flow that can be utilized in determining the distance-of-run to detonation. Moreover, as part of the SURF model [Menikoff and Shaw, 2010], a shock detector has been implemented in the `xRage` code. The shock detector is based on the Hugoniot energy condition and can be used with any HE model. It provides auxiliary information for the lead shock pressure (P_s) and shock arrival time as a function of position. This information is well suited to determining the run distance.

Figure 2 shows an example of the lead shock trajectory in both the (x, t)–plane and (P_s, x)–plane. Since the shock pressure $P_s(x)$ rises very rapidly at initiation, a simple threshold criterion can be used to define the run distance; first x such that $P_s(x) > P_{\text{threshold}}$. It is natural to choose a threshold pressure a little less than the CJ pressure of a propagating detonation wave. Moreover, varying $P_{\text{threshold}}$ can be used to estimate the uncertainty in the run distance.

In addition, P_s at the start of the shock trajectory defines the initial shock pressure in the HE. This is consistent with the EOS used in the simulation. It is very helpful since most hydro codes do not have option to provide the shock locus in the (P, u)–plane, which is needed to determine the initial shock pressure from the projectile velocity.

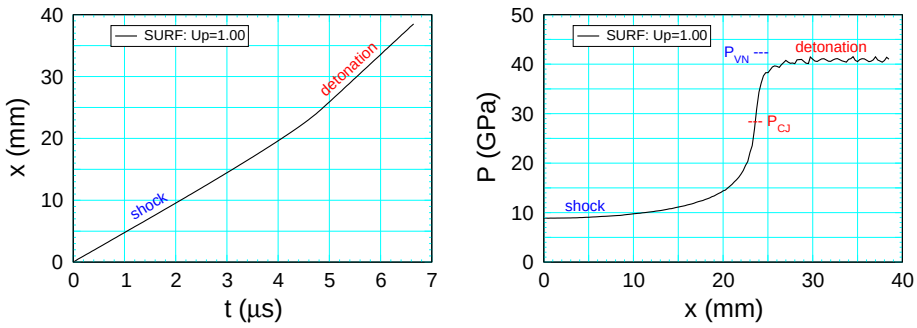

Figure 2: Trajectory of lead shock in (x, t)–plane and (P_s, x)–plane from a SDT simulation.

4 Automated computation of Pop plot

There are two parts to automating the computation of the Pop plot. The first is the directory structure for providing the information on the HE model to setup the SDT simulations. The second is scripts to generate the input file, run the simulations and post process the results. The run scripts takes advantage of the `xRage` code input parser which allows for include files.

Directory structure is as follows:

1. directory **input**
   Input file template, `SDT.input`, for SDT simulation. Template utilizes three include files:
   (a) `init.inc`
   Input parser parameters for level 1 cell size, length of material regions, and projectile velocity.
   (b) `material.inc`
   Specifies three materials; inert HE for projectile and buffer, reactants HE and products HE.
   Also specifies parameters for the adaptive mesh refinement(AMR) of each material.
   (c) `HE.inc`
   Specifies HE model and its associated paramerters.
2. subdirectory **HE/model**
   Include files to be used with input file template
   and subdirectory `teos` for data to generate `xRage` code tabular EOS.

Scripts utilize **Results** directory structure analogous to **input** directory; *i.e.*, each computed Pop plot is labeled by HE and model. In addition, output files for each simulation are in subdirectory labeled by particle velocity of initial HE shock `Ux.xx` where `x.xx` is half the projectile velocity. The directory structure facilitates comparing results for different HEs or models.

The scripts are as follows:

1. `runSDT`
   Generates input file in the **Results/HE/model/Ux.xx** directory and runs simulation for single point on Pop plot.

2. `SimulatePopPlot`
   Loops over list of projectile velocities and calls `runSDT` script for each. Then calls `ComparePopPlot` script to post process simulation output to generate Pop plot.

3. `ComparePopPlot`
   Loops over each simulation in the **Results/HE/model/U*** directories to generate points on Pop plot utilizing the shock detector output. Then generates plot comparing numerical and experimental run distance versus shock pressure and time-to-detonation versus shock pressure.

Other scripts are available to generate diagnostic information from dump files to provide checks that each simulation has run as intended, and if not to help diagnose the problem (which is usually an error in the input or EOS).

5 Illustrative examples

An HE model is composed of three parts: EOS of reactants, EOS of products and burn rate. Using PBX 9502 as the HE, the computation of the Pop plot is illustrated for three burn models: SURF [Menikoff and Shaw, 2010], WSD [Wescott et al., 2005], Forest Fire [Mader and Forest, 1976] (see also [Mader, 1979, p. 233])[1]. These models have previously been calibrated to fit the Pop plot data. We note that the burn models use different EOS for the HE, and have slightly different detonation speeds and Chapman-Jouguet (CJ) states due to the products EOS, and different von Neumann (VN) spike states due to the reactants EOS.

The calculated Pop plots of each model, both distance-of-run to detonation and time to detonation, are shown in figure 3. They are remarkably similar. This shows that different HE models can be used to fit Pop plot data. The figure also shows a slight variation with the value of $P_{\text{threshold}}$ used to determine the ignition point. With a higher threshold, the Pop plot shifts up, and the HE would appear to be slightly less sensitive. The variation is well within the experimental uncertainty; see [Gustavsen et al., 2006, fig. 10].

[1] X0290 was the development version that became PBX 9502.

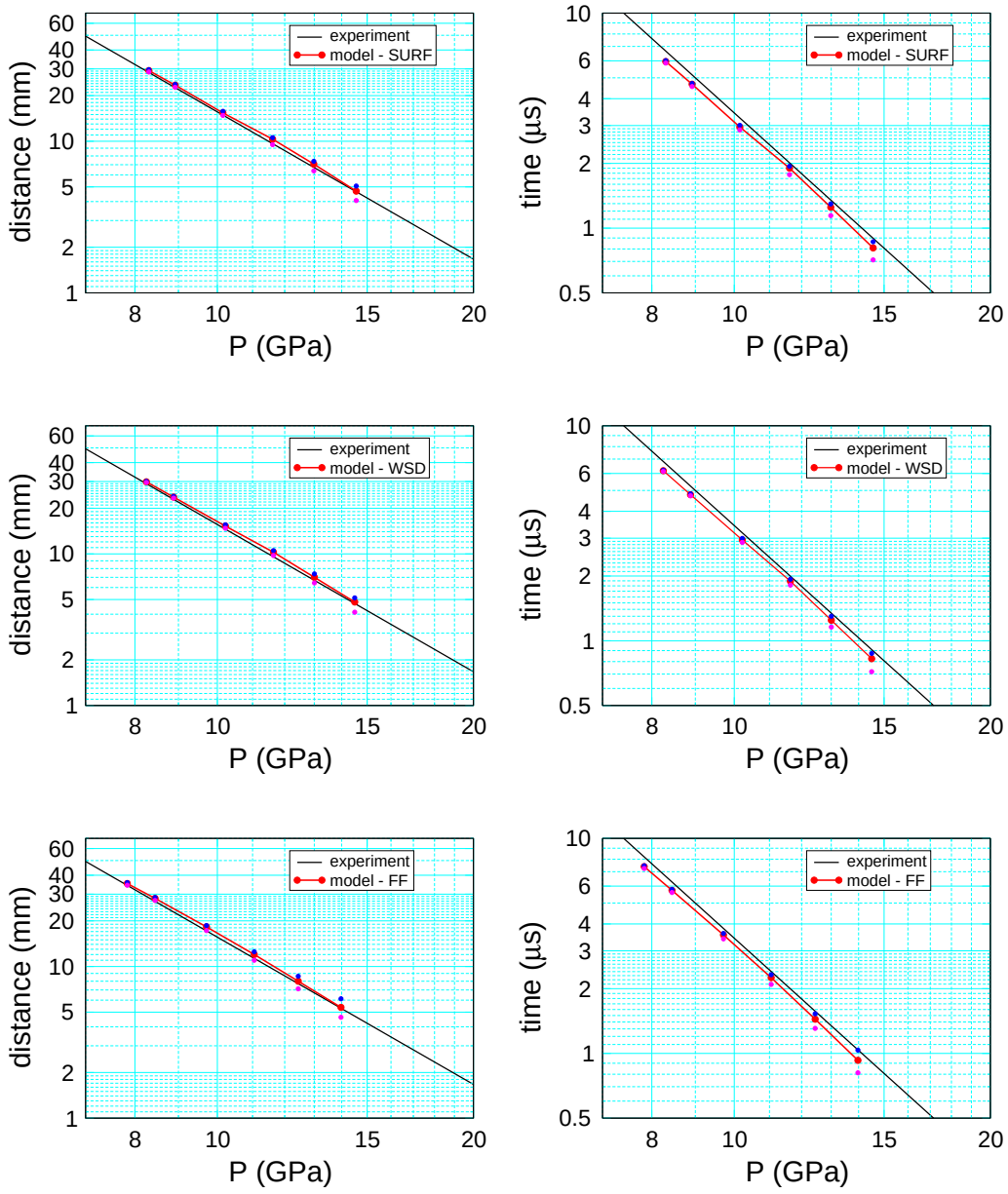

Figure 3: Comparison of experimental and numerical Pop plots for PBX 9502 using SURF, WSD and Forest Fire burn models. Magenta, red and blue circles use $P_{\text{threshold}} = 20, 25, 30\,\text{GPa}$, respectively. Experimental data from [Gibbs and Popolato, 1980, p. 125].

The SDT simulations for Pop plot points can be run in parallel on separate processors. On one node of *mapache*, using the typical resolution for HE simulations of $\frac{1}{8}$ mm, generating the Pop plot for one case (HE/model) takes about 5 minutes.

Profiles of the pressure and burn fraction just before ignition are shown in figure 4. Some of the differences stem from the different reactants EOS used by each model, which result in different shock pressures for the same projectile velocity. In addition, the log-log scale of the Pop plot reduces the apparent differences in the ignition point. To mitigate these effects, the simulation time for the profile plots were taken to correspond to when the peak pressure in each model is about 25 GPa.

We note that the calibration of the burn rate to the Pop plot can compensate for inaccuracies of the reactants EOS. However, significant discrepancies between SDT experiments and simulations using the actual projectile material and measured projectile velocity can occur due to the initial pressure match with an inaccurate reactants EOS.

Below the CJ pressure, the burn rate is modest and figure 4 shows that the reacting region is well resolved. Qualitative differences in the profiles are seen for the different models. Therefore, the Pop plot does not completely characterize shock initiation. With different drive conditions, *e.g.*, a pressure gradient as occurs in the gap test rather than a sustained shock from a projectile impact, one would expect the models to give different predictions for ignition.

Profiles of the pressure and burn fraction for the detonation wave at the end of the simulations are shown in figure 5. Due to the high burn rate, the propagating detonation wave has only 2 or 3 points for the fast part of the reaction zone. The WSD model has many more points for the slow part of the reaction zone. Extensions of the other two models, SURFplus [Menikoff and Shaw, 2012] and Forest Fire with buildup [Mader, 1979, sec. 2C] also have fast and slow reactions. These were not used since the Pop plot is determined predominantly by the fast reaction. The pressure profile behind the reaction zone is determined predominantly by the CJ isentrope of the products EOS. For a propagating detonation wave, the resolution mainly affects the numerical shock width which largely determines the curvature effect, detonation speed as function of local front curvature; see [Menikoff, 2014].

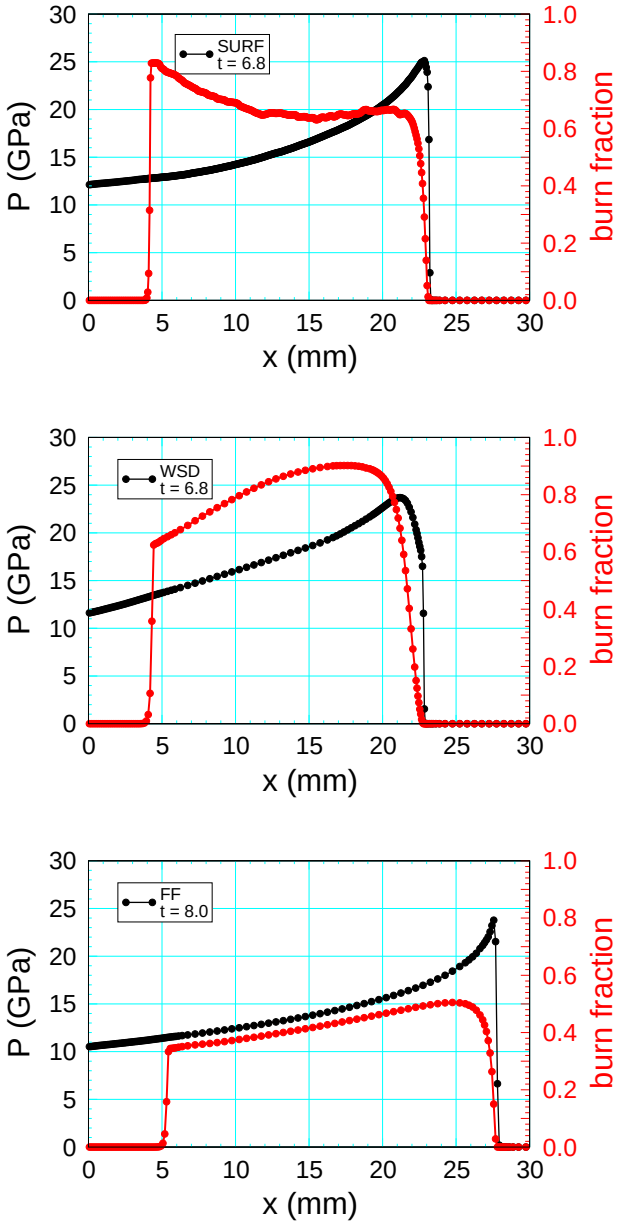

Figure 4: Pressure and burn fraction profiles just before ignition in PBX 9502 from SURF, WSD and Forest Fire burn model simulations with projectile velocity of 2 km/s.

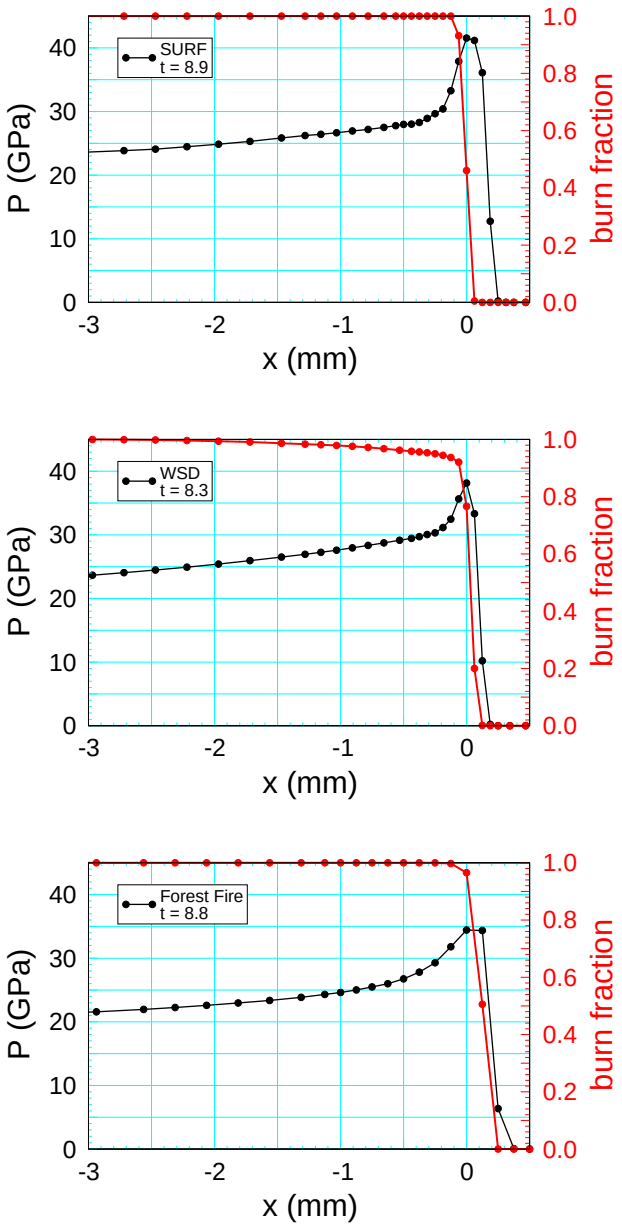

Figure 5: Pressure and burn fraction profiles for detonation wave in PBX 9502 from SURF, WSD and Forest Fire burn model simulations with projectile velocity of 2 km/s.

6 Calibration issues

The Forest Fire model is unique in that it is calibrated exclusively to Pop plot data. Moreover, the rate is determined by Forest's analysis which makes a number of assumptions; see [Mader, 1979, chpt. 4] or [Menikoff and Shaw, 2008]. The assumption of a reactive shock is difficult to enforce in a shock capturing algorithm; *e.g.*, bottom plot of figure 5 shows reactive shock overshooting CJ pressure. Another assumption of a zero pressure gradient behind the lead shock is only very approximate, see figure 4. The good fit to the Pop plot shown in figure 3 required scaling the derived Forest Fire rate by a factor of 0.8 .

All other rate models have a large number of parameters; up to two dozen for the WSD model. The Pop plot is not sensitive to many of the model parameters. This is not surprising since the Pop plot is characterized by only 2 parameters. Burn rates typically have one or more terms of the form $g(\lambda) \times f(P)$, where λ is the burn fraction and P is the local pressure. Some models, such as Ignition & Growth [Lee and Tarver, 1980] from which WSD is derived, take $f(P) = A \times P^n$. For the growth term of the fast reaction, the parameters A and n, with all other model parameters held fixed, can be fit to Pop data. Similarly, the SURF model rate is proportional to a factor of the form $f(P_s) = \exp(A + B \times P_s)$, where P_s is the lead shock pressure. Again with all other parameters held fixed, the parameters A and B can be fit to Pop plot data. Generally, one parameter dominates the slope (n or B) and the other parameter dominates the intercept (A).

Calibrating two appropriate model parameters to Pop plot data can be automated. First, one needs a metric for goodness of fit. It is natural to minimize the residual of the relative error in the run distance

$$residual = \sum_i \left[\frac{x_i - x_{pp}(P_i)}{x_{pp}(P_i)} \right]^2 , \tag{1}$$

where $x_{pp}(P_i)$ is the run distance from the Pop plot and x_i is the run distance from a simulation with the corresponding shock pressure P_i. To leading order, this corresponds to minimizing the distance on the log scale of the Pop plot; *i.e.*,

$$\begin{aligned} \log(x) - \log(x_{pp}) = \log(x/x_{pp}) &= \log\Big(1 + (x - x_{pp})/x_{pp}\Big) \\ &= \frac{x - x_{pp}}{x_{pp}} + \mathcal{O}\left(\left[\frac{x - x_{pp}}{x_{pp}} \right]^2 \right) . \end{aligned}$$

Then a fitting program can call the **SimultePopPlot** script to run the simulations and evaluate the residual.

The λ dependence of the rate affects the shape of the pressure profiles before ignition. Other data are needed to determine this dependence, such as embedded velocity gauge data [Gustavsen et al., 2006]. To have confidence in the fitting form used for the rate model, data for other drive conditions would be very useful; such as short shock, multiple shock or a shock followed by a pressure gradient as occurs in the gap test; see for example [Gibbs and Popolato, 1980, part II, sec 4.2].

The data to calibrate and validate models should be available to all modelers. A natural place for the data is the small scale database at LANL; `http://smallscale.lanl.gov`. In addition to the experimental data, meta-data is included to make the data files self contained. This facilitates automating simulations and comparison with experiment; see for example [Menikoff and Scovel, 2012].

There are several issues with utilizing a fitting program to calibrate simultaneously all model parameters. First, one needs a metric for goodness of fit that appropriately weights different types of data and the uncertainty in the data from different experiments. Second, the fits are highly non-linear, and fitting programs use iterative algorithms to minimize the metric. Constraints are needed for model parameters to stay within an appropriate domain in order for the iterations to converge to a local minimum. Then there is the problem of finding the best local minimum.

A path forward is to automate simulations for classes of experiments. These can be run with select model parameters to gain intuition on how to constrain the parameter domain and the most efficient order in which to vary the parameters. This is especially important since evaluating the metric involves many hydro code simulations and is computationally expensive.

7 Final remarks

The scripts discussed in sec. 4 along with the input directory to generate the illustrative example plots of sec. 5 are available on the `xRage` svn repository under the directory `Test.rh/Nobel/HE_PopPlot`. A `README` file gives a brief description of how to use the scripts.

The same methodology can be applied to other hydro codes. The shock detector utilized to determine the run distance would need to be implemented. Since most codes do not have the equivalent of the `xRage` input parser, the run script would have to generate the input file by substituting the include files into the input file template. Finally, the input template and the include files would have to be modified to be compatible with the form of input that the hydro code utilizes.

References

T. R. Gibbs and A. Popolato, editors. *LASL Explosive Property Data*. Univ. of Calif. Press, 1980. URL http://library.lanl.gov/ladcdmp/epro.pdf. 2, 7, 12

R. L. Gustavsen, S. A. Sheffield, R. R. Alcon, and L. G. Hill. Shock initiation of new and aged PBX 9501. In *Proceeding of the Twelfth International Symposium on Detonation*, pages 530–537, 2002. 2

R. L. Gustavsen, S. A. Sheffield, and R. R. Alcon. Measurements of shock initiation in the TATB based explosive PBX 9502: Wave forms from embedded gauges and comparison of four different material lots. *J. Appl. Phys.*, 99:114907, 2006. 6, 12

L. G. Hill and R. L. Gustavsen. On the characterization of mechanisms of shock initiation in heterogeneous explosives. In *Proceeding of the Twelfth International Symposium on Detonation*, pages 975–984, 2002. 4

E. L. Lee and C. M. Tarver. Phenomenological model of shock initiation in heterogeneous explosives. *Phys. Fluids*, 23:2362–272, 1980. 11

C. L. Mader. *Numerical Modeling of Detonation*. Univ. of Calif. press, first edition, 1979. 6, 8, 11

C. L. Mader and C. A. Forest. Two-dimensional homogeneous and heterogeneous detonation wave propagation. Technical Report LA-6259, Los Alamos Scientific Laboratory, 1976. URL http://library.lanl.gov/cgi-bin/getfile?00322771.pdf. 6

R. Menikoff. Errors when shock waves interact due to numerical shock width. *SIAM J. Sci. Comput.*, 15, 1994. 3

R. Menikoff. Effect of resolution on propagating detonation wave. Technical Report LA-UR-14-25140, Los Alamos National Laboratory, 2014. URL http://dx.doi.org/10.2172/1136940. 8

R. Menikoff and C. A. Scovel. Systematic approach to verification and validation: High explosive burn models. Technical Report LA-UR-12-20591, Los Alamos National Laboratory, 2012. URL http://www.osti.gov/scitech/servlets/purl/1038871. 12

R. Menikoff and M. S. Shaw. Review of the Forest Fire model for high explosives. *Combustion Theory and Modelling*, 12:569–604, 2008. 11

R. Menikoff and M. S. Shaw. Reactive burn models and Ignition & Growth concept. *EPJ Web of Conferences*, 10, 2010. URL http://dx.doi.org/10.1051/epjconf/20101000003. 4, 6

R. Menikoff and M. S. Shaw. The SURF model and the curvature effect for PBX 9502. *Combustion Theory And Modelling*, pages 1140–1169, 2012. URL http://dx.doi.org/10.1080/13647830.2012.713994. 8

J. B. Ramsay and A. Popolato. Analysis of shock wave and initiation data for solid explosives. In *Proceeding of the Fourth International Symposium on Detonation*, pages 233–238, 1965. 2

B. L. Wescott, D. S. Stewart, and W. C. Davis. Equation of state and reaction rate for condensed-phase explosives. *J. Appl. Phys.*, 98:053514, 2005. 6